LETTERS

Clumps and streams in the local dark matter distribution

J. Diemand[1], M. Kuhlen[2], P. Madau[1], M. Zemp[1], B. Moore[3], D. Potter[3] & J. Stadel[3]

In cold dark matter cosmological models[1,2], structures form and grow through the merging of smaller units[3]. Numerical simulations have shown that such merging is incomplete; the inner cores of haloes survive and orbit as 'subhaloes' within their hosts[4,5]. Here we report a simulation that resolves such substructure even in the very inner regions of the Galactic halo. We find hundreds of very concentrated dark matter clumps surviving near the solar circle, as well as numerous cold streams. The simulation also reveals the fractal nature of dark matter clustering: isolated haloes and subhaloes contain the same relative amount of substructure and both have cusped inner density profiles. The inner mass and phase-space densities of subhaloes match those of recently discovered faint, dark-matter-dominated dwarf satellite galaxies[6-8], and the overall amount of substructure can explain the anomalous flux ratios seen in strong gravitational lenses[9,10]. Subhaloes boost γ-ray production from dark matter annihilation by factors of 4 to 15 relative to smooth galactic models. Local cosmic ray production is also enhanced, typically by a factor of 1.4 but by a factor of more than 10 in one per cent of locations lying sufficiently close to a large subhalo. (These estimates assume that the gravitational effects of baryons on dark matter substructure are small.)

The cold dark matter (CDM) model has been remarkably successful at describing the large-scale mass distribution of our Universe from the hot Big Bang to the present. However, the nature of the dark matter particle is best tested on small scales, where its interaction properties manifest themselves by modifying the structure of galaxy haloes and their substructures. CDM theory predicts that the growth of cosmic structures begins early, on Earth-like mass scales[11,12], and continues from the bottom up until galaxy clusters form that are 20 orders of magnitude more massive. Resolving small-scale structures is extremely challenging, as the range of lengths, masses, and timescales that need to be simulated is immense. We have performed the highest precision calculation—which we name Via Lactea II—of the assembly of the Galactic CDM halo. The simulation follows the growth of a Milky Way-size system from redshift 104.3 to the present. It provides the most accurate predictions on the small-scale clustering of dark matter so far available and puts constraints on the local subhalo abundance and properties. We used the parallel tree-code PKDGRAV2 (ref. 13) and sampled a galaxy-forming region with 1.1×10^9 particles of mass $4,100 M_\odot$ (where $M_\odot$ denotes the mass of the Sun). Cosmological parameters were taken from Wilkinson Microwave Anisotropy Probe data[14]; see the Supplementary Information for more details and a comparison with our previous simulation[15] of the Galactic CDM halo, Via Lactea.

The wealth of substructure that survives the hierarchical assembly process until the present epoch is clearly seen in Fig. 1: we resolve over 40,000 subhaloes within 402 kpc of the centre and find that they are distributed with approximately equal total mass in subhaloes per

decade of mass over the range $10^6 M_\odot$–$10^9 M_\odot$. They have very high central phase-space densities ($\gtrsim 10^{-5} M_\odot \, \mathrm{pc}^{-3} \, \mathrm{km}^{-3} \, \mathrm{s}^3$) owing to their steep inner density cusps and their relatively small internal velocity dispersions. This agrees well with the extremely high phase-space densities inferred from stellar motions within ultrafaint dwarf galaxies[7]. Our predicted inner subhalo densities ($0.4 M_\odot$–$2.5 M_\odot \, \mathrm{pc}^{-3}$ within 100 pc of centre, $7 M_\odot$–$46 M_\odot \, \mathrm{pc}^{-3}$ within 10 pc of centre) are also in excellent agreement with the observations[6,7]. The fact that CDM theory naturally predicts a small-scale
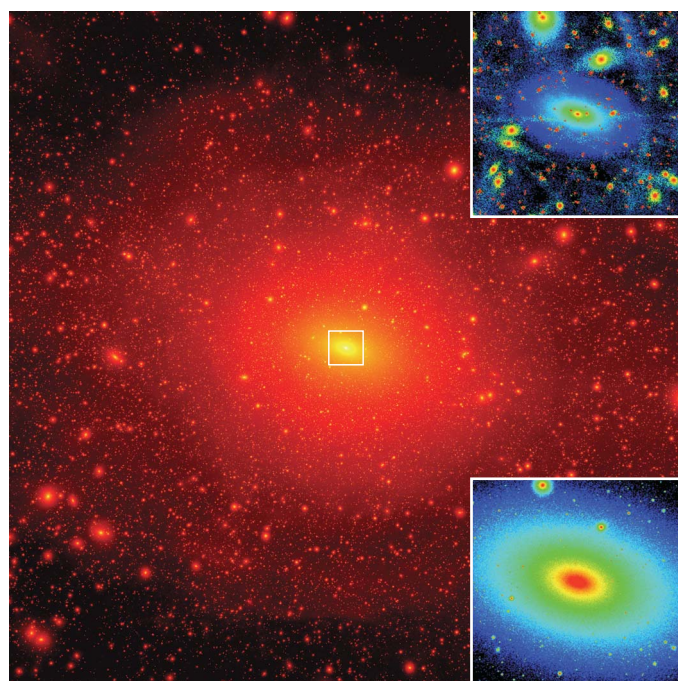
Figure 1 | Via Lactea II projected dark matter squared-density map. A cube of 800 kpc per side is shown. The insets focus on an inner cube of 40 kpc per side (outlined in white), and show local density (bottom inset) and local phase-space density calculated with EnBiD (ref. 27; top inset). The Via Lactea II simulation has a mass resolution of $4,100 M_\odot$ and a force resolution of 40 pc. It used over a million processor hours on the 'Jaguar' Cray XT3 supercomputer at the Oak Ridge National Laboratory. A new method was employed to assign physical, adaptive time steps[19] equal to 1/16 of the local dynamical timescale (but not less than 268,000 yr), which enables the resolution of very high-density regions. Initial conditions were generated with a modified, parallel version of GRAFIC2 (ref. 28). The high-resolution region is embedded within a large periodic box (40 co-moving megaparsecs) to account for the large-scale tidal forces. The mass within $r_{200} = 402$ kpc of the centre (the radius enclosing 200 times the mean matter density) is $1.9 \times 10^{12} M_\odot$.

[1]University of California, Department of Astronomy and Astrophysics, Santa Cruz, California 95064, USA. [2]Institute for Advanced Study, Einstein Drive, Princeton, New Jersey 08540, USA. [3]University Zurich, Institute for Theoretical Physics, Winterthurerstrasse 190, 8057 Zurich, Switzerland.

dark matter distribution that matches the observations is a real success of the model. Particle candidates that introduce a low phase-space limit, such as a sterile neutrino, or that have a high collisional cross-section, such as self-interacting dark matter, would fail these fundamental observational tests.

The phase-space map (Fig. 1, upper inset) contains coherent elongated features. These are streams which form from material removed from accreted and disrupted subhaloes. The few visible streams have quite low densities (about 100 times below the local density), but owing to their low velocity dispersion (which is about 10 times smaller than that of background particles) they can just be distinguished by their local phase-space densities (which are about $10^{-9} M_\odot \, \mathrm{pc}^{-3} \, \mathrm{km}^{-3} \, \mathrm{s}^3$). These resolved streams, together with the multitude of expected finer-grained phase-space structures that we currently cannot resolve, will lead to unique signatures in direct detection experiments, especially those with directional sensitivity. In cases where the disrupted subhalo hosts a luminous satellite galaxy, the resulting streams will contain not only dark matter but also stars. This process will then produce detectable features in the Milky Way's stellar halo, like those observed in the 'field of streams'[16].

Further evidence for halo substructure comes from the anomalous flux ratios in multiply imaged gravitationally lensed quasars[17,18]. Perturbations of the light path caused by substructure can explain this phenomenon if the projected substructure fraction within 10 kpc of the centre is about 1% (refs 9,10). Within a projected distance of 10 kpc from the centre, 0.50% of the host mass belongs to resolved substructure, which could be just enough to explain the observed flux anomalies. In earlier simulations this percentage was lower; the halo simulated by Via Lactea[15] predicted only 0.25%, indicating that this quantity has not yet converged in the simulations.

Via Lactea II predicts a remarkable self-similar pattern of clustering properties: our simulation integrates particle orbits extremely accurately in high-density regions[19], allowing a precise determination of the density profile within the inner kiloparsecs of the Galactic halo and within the centres of its satellite galaxies. We find that a cusped profile fits the host halo's density profile well, whereas the best-fit profile with a core lies below the simulated inner densities (Fig. 2). The inner profiles of subhaloes are also consistent with the presence of cusps over their resolved ranges. They scatter around the moderate cusp index of the host halo ($\gamma = 1.24$): some of them are denser in the inner part, and some are less dense, exactly like the inner parts of field haloes, which have inner slopes of $\gamma \approx 1.2 \pm 0.2$ (ref. 20). At large radii, subhalo density profiles generally fall off faster than field halo profiles. These similarities and differences between subhalo and field halo profiles have a simple explanation: subhalo density profiles were modified by tidal mass loss, which removes material from the outside in, but does not change the inner cusp structure[15,21]. Figure 3 shows that the dwarf satellites of the Milky Way appear to be scaled versions of the main halo not only in their inner mass distribution, but also in term of relative substructure abundances. Via Lactea II demonstrates the fractal-like appearance of the dark matter by resolving the second generation of surviving sub-substructures from the merging hierarchy. This suggest that at infinite resolution we would find a long nested series of haloes within haloes within haloes, and so forth, reminiscent of a Russian doll, all the way down the first and smallest Earth-mass haloes that form.

The multitude of dark substructures increases the dark matter annihilation signal, as it is proportional to the square of the local density. For cusped profiles (Fig. 2) with some fixed inner slope ($\gamma < 1.5$) we find the following simple scaling relation for the annihilation:

$$L \propto \rho_s^2 r_s^3 \propto V_{max}^4 / r_{V_{max}} \propto V_{max}^3 \sqrt{c_V}$$

(see the Supplementary Information for the definition of the concentration c_V and its values). In combination with the steep subhalo velocity function $N(> V_{max}) \propto V_{max}^{-3}$, this implies that subhaloes of all sizes contribute about equally to the total signal coming from the

Galactic dark halo. Taking the higher concentrations of smaller systems[22] into account, we find that small subhaloes contribute more than large ones[23,24]. Summing the values of $V_{max}^4 / r_{V_{max}}$ for all the resolved subhaloes in Via Lactea II gives a number close (97%) to the host halo's $V_{max}^4 / r_{V_{max}}$ value; that is, the resolved subhaloes already contribute as much as their smooth host would alone. In other words, the 'substructure boost factor' is at least 1.97. Extrapolating down to microsubhaloes of size $V_{max} = 0.25 \, \mathrm{m \, s}^{-1}$, taking into account how concentrations depend on subhalo size[22] and position (see the Supplementary Information), and assuming a uniform distribution of subhalo inner slopes α between 1.0 and 1.5 leads to a total boost factor of 14.6. Most of it comes from very small clumps: halting the same extrapolation at $V_{max} = 44 \, \mathrm{m \, s}^{-1}$ lowers the boost factor to 6.6. Although the contribution from small, dark clumps is not affected by baryons, it may not dominate the total signal in situations in which baryonic collapse greatly increases the central dark matter densities in larger haloes. However, the net effect of stars, black holes and galaxy formation is unclear, and it may actually lead to a reduction in the central dark matter densities.
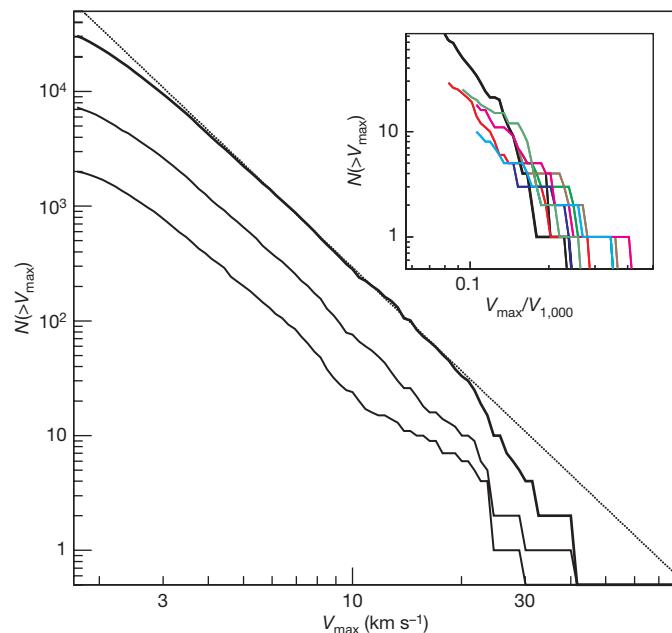
The detailed distribution of cusp indices is still unknown, because only a few haloes have been simulated with sufficient resolution[20]. For the annihilation boost factors the existence of a few steep cusps
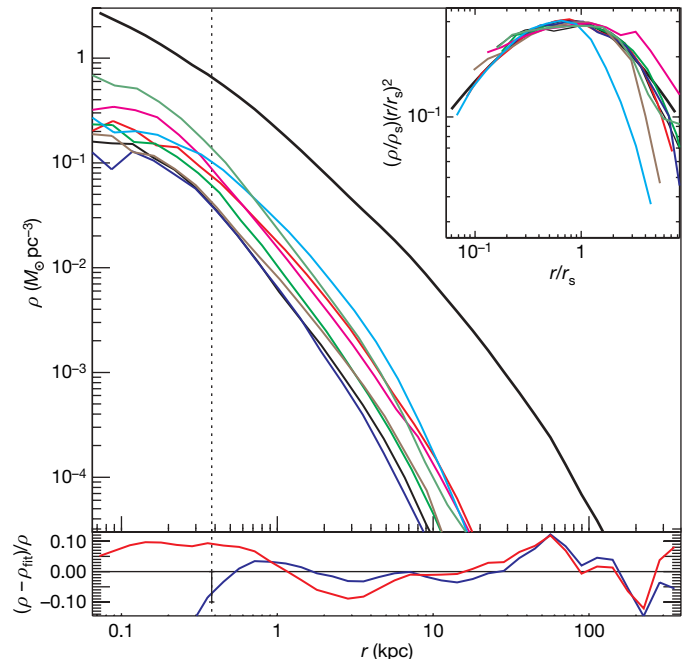
Figure 2 | Density profiles of main halo and subhaloes. Main panel, profile of the Milky Way halo (thick line) and of eight large subhaloes (thin lines). Lower panel, the relative differences between the simulated main halo profile and a fitting formula with a core[29], $\rho(r) = \rho_s \exp(-2/\alpha[(r/r_s)^\alpha - 1])$ (best-fit parameters $\alpha = 0.170$, $r_s = 21.5$ kpc, $\rho_s = 1.73 \times 10^{-3} M_\odot \, \mathrm{pc}^{-3}$; red curve), and one with a cusp[20], $\rho(r) = \rho_s (r/r_s)^{-\gamma} (r/r_s + 1)^{-3+\gamma}$ (best-fit inner slope $\gamma = 1.24$, $r_s = 28.1$ kpc, $\rho_s = 3.50 \times 10^{-3} M_\odot \, \mathrm{pc}^{-3}$; blue curve). The vertical dotted line indicates the estimated convergence radius of 380 pc: simulated local densities are only lower limits within this radius and should be correct to within 10% at this radius (vertical error bar) and outside it. The cusped profile is a good fit to the inner halo, whereas the profile with a core has too shallow a slope in the inner few kiloparsecs, causing it to overestimate densities around 4 kpc and to underestimate them at all radii less than 1 kpc. The simulated densities are higher than the best-fit profile with a core even at 80 pc, where they are certainly underestimated owing to numerical limitations. We find the same behaviour in the inner few kiloparsecs in all six snapshots that we have analysed so far between redshifts $z = 3$ and $z = 0$. The large residuals in the outer haloes, on the other hand, are transient features; they are different in every snapshot. Inset, rescaled host halo (thick line) and subhalo (thin lines) density profiles multiplied by squared radius to reduce the vertical range of the figure.

near $\gamma = 1.5$ would make a big difference, because the signal diverges logarithmically towards the centre in a $\gamma = 1.5$ cusp. Cutting the assumed uniform distribution of inner slopes at $\gamma = 1.4$ instead of $\gamma = 1.5$ gives boost factors of 9.9 instead of 14.6 and 4.3 instead of 6.6. These factors imply that most of the extra-Galactic γ-ray background from dark matter annihilation[23], which will be constrained or even detected by the upcoming Gamma-ray Large Area Space Telescope mission, should be emitted by subhaloes, and not by distinct host haloes.

As well as γ-rays, dark matter annihilation would produce charged particles and antiparticles that, owing to magnetic field entanglement, propagate over much shorter distances within the Galaxy. Space-based experiments (like the Payload for Antimatter Matter Exploration and Light-nuclei Astrophysics mission and, in the near future, the Alpha Magnetic Spectrometer experiment AMS-02) could detect antiparticles produced in dark matter annihilations within about 1 kpc of the centre[25]. To determine what fraction of this local annihilation would happen in nearby subhaloes, we constrain the local boost factor using the same assumptions as above ($\gamma = 1$–1.5, $V_{max} \geq 0.25\ \mathrm{m\ s^{-1}}$), but now we only include subhaloes within 1 kpc of the solar system (see the Supplementary Information for the local

subhalo abundance). The resulting signal is 40% of the smooth halo signal, giving a boost factor of 1.4, which we estimated using the spherically averaged density at 8 kpc ($\rho_0 = 0.40\ \mathrm{GeV}\ c^{-2}\ \mathrm{cm^{-3}}$, where c denotes the speed of light). Explaining the positron excess from the High-Energy Antimatter Telescope experiment[26] with local dark matter annihilation requires boost factors of about 3 to 100 (ref. 25). When a relatively large subhalo happens to lie within 1 kpc of the Solar System, the higher boost factors can be achieved without violation of the local subhalo constraints from our simulation. Such cases are possible, but are not likely to occur: only 5.2% of all random realizations have a boost factor ≥ 3 (caused by there being a clump with $V_{max} \geq 3.4\ \mathrm{km\ s^{-1}}$ within 1 kpc of the Solar System). In only 1.0% of the cases, the boost factor is ≥ 10, owing to a nearby, large-V_{max} ($\geq 5.6\ \mathrm{km\ s^{-1}}$) subhalo.

1. Peebles, P. J. E. Large-scale background temperature and mass fluctuations due to scale-invariant primeval perturbations. *Astrophys. J.* **263**, L1–L5 (1982).
2. Blumenthal, G. R., Faber, S. M., Primack, J. R. & Rees, M. J. Formation of galaxies and large-scale structure with cold dark matter. *Nature* **311**, 517–525 (1984).
3. White, S. D. M. & Rees, M. J. Core condensation in heavy halos - A two-stage theory for galaxy formation and clustering. *Mon. Not. R. Astron. Soc.* **183**, 341–358 (1978).
4. Ghigna, S. *et al.* Dark matter haloes within clusters. *Mon. Not. R. Astron. Soc.* **300**, 146–162 (1998).
5. Klypin, A., Kravtsov, A. V., Valenzuela, O. & Prada, F. Where are the missing galactic satellites? *Astrophys. J.* **522**, 82–92 (1999).
6. Strigari, L. E. *et al.* The most dark matter dominated galaxies: Predicted gamma-ray signals from the faintest milky way dwarfs. *Astrophys. J.* **678**, 614–620 (2008).
7. Simon, J. D. & Geha, M. The kinematics of the ultra-faint milky way satellites: Solving the missing satellite problem. *Astrophys. J.* **670**, 313–331 (2007).
8. Belokurov, V. *et al.* Cats and dogs, hair and a hero: A quintet of new milky way companions. *Astrophys. J.* **654**, 897–906 (2007).
9. Dalal, N. & Kochanek, C. S. Direct detection of cold dark matter substructure. *Astrophys. J.* **572**, 25–33 (2002).
10. Metcalf, R. B., Moustakas, L. A., Bunker, A. J. & Parry, I. R. Spectroscopic gravitational lensing and limits on the dark matter substructure in Q2237+0305. *Astrophys. J.* **607**, 43–59 (2004).
11. Green, A. M., Hofmann, S. & Schwarz, D. J. The power spectrum of SUSY-CDM on subgalactic scales. *Mon. Not. R. Astron. Soc.* **353**, L23–L27 (2004).
12. Diemand, J., Moore, B. & Stadel, J. Earth-mass dark-matter haloes as the first structures in the early Universe. *Nature* **433**, 389–391 (2005).
13. Stadel, J. G. *Cosmological N-body Simulations and Their Analysis.* PhD thesis, Univ. Washington (2001).
14. Spergel, D. N. *et al.* Three-year Wilkinson Microwave Anisotropy Probe (WMAP) observations: Implications for cosmology. *Astrophys. J. Suppl. Ser* **170**, 377–408 (2007).
15. Diemand, J., Kuhlen, M. & Madau, P. Formation and evolution of galaxy dark matter halos and their substructure. *Astrophys. J.* **667**, 859–877 (2007).
16. Belokurov, V. *et al.* The field of streams: Sagittarius and its siblings. *Astrophys. J.* **642**, L137–L140 (2006).
17. Mao, S. & Schneider, P. Evidence for substructure in lens galaxies? *Mon. Not. R. Astron. Soc.* **295**, 587–594 (1998).
18. Metcalf, R. B. & Madau, P. Compound gravitational lensing as a probe of dark matter substructure within galaxy halos. *Astrophys. J.* **563**, 9–20 (2001).
19. Zemp, M., Stadel, J., Moore, B. & Carollo, C. M. An optimum time-stepping scheme for N-body simulations. *Mon. Not. R. Astron. Soc.* **376**, 273–286 (2007).
20. Diemand, J., Moore, B. & Stadel, J. Convergence and scatter of cluster density profiles. *Mon. Not. R. Astron. Soc.* **353**, 624–632 (2004).
21. Kazantzidis, S. *et al.* Density profiles of cold dark matter substructure: Implications for the missing-satellites problem. *Astrophys. J.* **608**, 663–679 (2004).
22. Bullock, J. S. *et al.* Profiles of dark haloes: evolution, scatter and environment. *Mon. Not. R. Astron. Soc.* **321**, 559–575 (2001).
23. Ullio, P., Bergström, L., Edsjö, J. & Lacey, C. Cosmological dark matter annihilations into γ rays: A closer look. *Phys. Rev. D* **66**, 123502 (2002).
24. Colafrancesco, S., Profumo, S. & Ullio, P. Multi-frequency analysis of neutralino dark matter annihilations in the Coma cluster. *Astron. Astrophys.* **455**, 21–43 (2006).
25. Lavalle, J., Yuan, Q., Maurin, D. & Bi, X. Full calculation of clumpiness boost factors for antimatter cosmic rays in the light of ΛCDM N-body simulation results. *Astron. Astrophys.* **479**, 427–452 (2008).
26. Beatty, J. J. *et al.* New measurement of the cosmic-ray positron fraction from 5 to 15GeV. *Phys. Rev. Lett.* **93**, 241102 (2004).
27. Sharma, S. & Steinmetz, M. Multidimensional density estimation and phase-space structure of dark matter haloes. *Mon. Not. R. Astron. Soc.* **373**, 1293–1307 (2006).

Figure 3 | Subhalo and sub-subhalo abundances. Number of subhaloes above V_{max} within $r_{200} = 402\ \mathrm{kpc}$ (thick solid line) and within 100 and 50 kpc of the galactic centre (thin solid lines, from top to bottom). V_{max} is the peak height of the subhalo circular velocity $v_{circ} = \sqrt{GM(<r)/r}$, where $M(<r)$ is the mass enclosed within a sphere of radius r and G is the gravitational constant. V_{max} serves as a simple proxy for the mass of a subhalo. The dotted line is $N(>V_{max}) = 0.036(V_{max}/V_{max,host})^{-3}$, where $V_{max,host} = 201\ \mathrm{km\ s^{-1}}$ (at $r_{V_{max,\ host}} = 60\ \mathrm{kpc}$). It fits the subhalo abundance above $V_{max} \approx 3.5\ \mathrm{km\ s^{-1}}$. The number of smaller subhaloes is artificially reduced by numerical limitations. Within r_{200} this halo has 1.7 times more substructure than the first Via Lactea halo[15], a factor well within the halo-to-halo scatter[30]. Within 50 kpc this grows to a factor of 2.6, probably because of the improved mass and time resolution of Via Lactea II, which enables better resolution of inner substructure. Inset, sub-subhalo abundance within $r_{1,000}$ (enclosing 1,000 times the mean matter density) of the centres of eight large subhaloes (those in Fig. 2; thin solid lines). $r_{1,000}$ is well inside the tidal radius for these systems. The thick solid line shows the subhalo abundance of the host halo inside its $r_{1,000}$, which equals 213 kpc. The subhalo and sub-subhalo V_{max} values are given in units of the $V_{1,000} = \sqrt{GM(<r_{1,000})/r_{1,000}}$ of the corresponding host halo or, respectively, subhalo. Lines stop at $V_{max} = 2\ \mathrm{km\ s^{-1}}$. The mean sub-substructure abundance is consistent with the scaled-down version of the main halo, and both the mean abundance and the scatter agree with results in ref. 30 for distinct field haloes.

28. Bertschinger, E. Multiscale Gaussian random fields and their application to cosmological simulations. *Astrophys. J. Suppl. Ser.* **137**, 1–20 (2001).

29. Navarro, J. F. *et al.* The inner structure of ΛCDM haloes - III. Universality and asymptotic slopes. *Mon. Not. R. Astron. Soc.* **349**, 1039–1051 (2004).

30. Reed, D. *et al.* Dark matter subhaloes in numerical simulations. *Mon. Not. R. Astron. Soc.* **359**, 1537–1548 (2005).